1. Aleksandra KUCHARCZYK-DRAB, 2. Radosław RYNIEC, 3. Marek PISZCZEK

Military University of Technology, Institute of Optoelectronics
ORCID: 1. 0000-0002-3821-5918; 2.000-0002-4090-0092, 3. 0000-0003-3376-6427

doi:10.15199/48.2025.02.54

Experimental measurement setup for hyperspectral mapping of diffuse radiation from the hemispheric sky

Abstract. *This paper presents the concept of a mobile, low-cost measurement station and methodology to derive a function that modifies the diffuse radiation model of the sky in real time, adjusting for current weather conditions. The experimental measurement setup is designed to capture both image data and associated metadata. The synthesis and processing of panoramic images from various sources and their analysis within a common coordinate framework demonstrate the effectiveness of this approach..*

Streszczenie. *Artykuł przedstawia koncepcję mobilnej, niskokosztowej stacji pomiarowej oraz metodologię opracowywania funkcji modyfikującej model rozproszonego promieniowania nieba w czasie rzeczywistym, uwzględniając aktualne warunki atmosferyczne. Eksperymentalna konfiguracja pomiarowa została zaprojektowana do rejestrowania zarówno danych obrazowych, jak i powiązanych metadanych. Syntetyzowanie i przetwarzanie panoramicznych obrazów z różnych źródeł oraz ich analiza w ramach wspólnego układu współrzędnych wykazują skuteczność tego podejścia. (**Eksperymentalne stanowisko pomiarowe do mapowania hiperspektralnego promieniowania rozproszonego z nieba półkulistego**)*

Keywords: solar radiation, spectral hypercube, image processing, data fusion
Słowa kluczowe: promieniowanie słoneczne, hipersześcian widmowy, przetwarzanie obrazów, fuzja danych

Introduction

In contemporary research, the investigation of the visible portion of the sky from a given location, known as the 'sky hemisphere,' is studied by several scientific disciplines, including astronomy and astrophysics (examining the behavior of stars and planets), meteorology and climatology (analyzing atmospheric circulation and weather patterns), geophysics (studying the Earth's magnetosphere and ionosphere), and atmospheric and environmental sciences (focusing on atmospheric optics and light scattering phenomena). The sky hemisphere also provides an environment for research into the detection and classification of various objects. Automation in these processes has become increasingly important in numerous applications. Such studies not only facilitate the understanding of remote cosmic phenomena but also contribute to meteor detection, the analysis of atmospheric entry effects, and impact risk assessment. The ability to monitor objects of terrestrial origin is particularly critical, including satellite tracking, the management of 'space debris,' and other objects in Earth's orbit (important for collision avoidance), as well as air traffic management—especially near airports and within flight corridors—where object detection, such as drones, is essential for ensuring the safe navigation of aircraft. Additionally, monitoring the sky for the detection of unidentified or potentially hostile aircraft, drones, or missiles supports national security initiatives, while identifying migratory bird patterns and other ecological phenomena is crucial for environmental monitoring and biodiversity studies. For tropospheric objects, the sky hemisphere serves as a highly variable environment (across a broad electromagnetic spectrum), influenced by factors such as weather conditions and the concentration and type of aerosols. From the perspective of scene analysis algorithms, it is advantageous for an object to exhibit distinctive characteristics against this dynamic background. This means that the sky's luminance becomes a reference parameter for analyzing the variability in object-background contrast, both at different levels of background complexity and across various spectral ranges..

Procedures and techniques for object detection, recognition, and identification are implemented through both active and passive systems, including radar, LIDAR, spectroscopic instruments, and vision-based systems. The computational tools employed may leverage fundamental image processing and computer vision libraries, as well as advanced deep learning models.

To achieve the long-term objective of automated object detection and classification in aerial contexts, the authors propose the use of simulation methods to evaluate the feasibility of passive, selective spectral imaging solutions, with the aim of future practical application. In this approach, model-derived data serve as a reference framework, which is iteratively refined based on empirical measurement data. The operational concept of the proposed system is schematically presented in Figure 1.

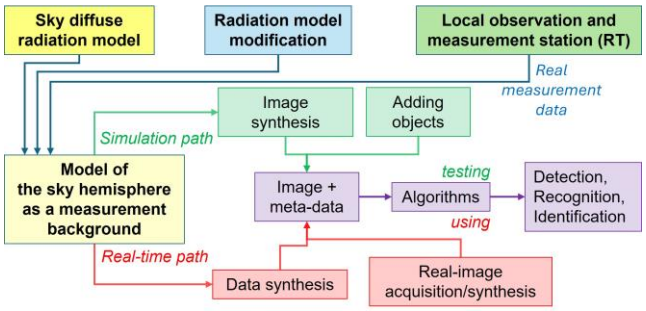

Fig. 1. Concept of functioning of the whole system for detection and recognition of objects in the sky background

The foundation of this approach is rooted in the use of established models of diffuse sky hemisphere radiation. The atmospheric radiation transfer model, which treats the atmosphere as an absorbing, scattering, and emitting medium, has been extensively studied over several decades [1–4]. These research had led to the development of standard atmospheric and radiation transfer models of varying levels of complexity. These models typically originate from the spectral distribution of extraterrestrial solar radiation, obtained from empirical data collected on multiple platforms.

A significant limitation of the models mentioned is the inadequate consideration of cloud effects, which can vary considerably depending on cloud type, spatial distribution and other factors affecting different regions of the sky hemisphere [5–16]. While these models do not directly supply the necessary data for such conditions, it is feasible to enhance their functionality through the integration of supplementary measurement data.

To overcome the mentioned limitation, this project proposes two key initiatives: the development of a dedicated hemispheric sky observation and measurement station, and the exploration of methodologies - including machine learning techniques - to provide a function that modifies the hemispheric diffuse radiation model in real time, adaptive to current weather conditions. The implementation of this concept is illustrated in Figure 2

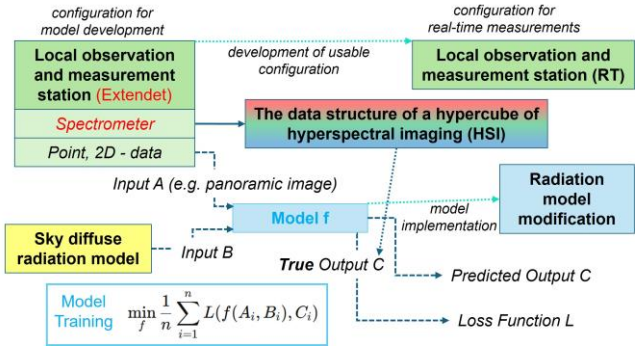

Fig. 2. Key Aspects of Task Implementation

The current developments focus on essential components related to the near-term objectives, particularly the creation of an experimental prototype of a local observation and measurement station, which includes a spectrometer. Additionally, efforts are directed toward the preparation and validation of measurement data for machine learning applications. The ultimate objective of employing machine learning in this context is to enhance the diffuse radiation model of the sky hemisphere, enabling it to account for real-time weather conditions.

An experimental measurement setup has been constructed to collect these data, primarily utilizing low-cost, commercially available components, such as various sensors and image sensors [13,14]. This paper presents the design of the measurement setup, initial results, and preliminary data processing, including the synthesis of panoramic images and a "spectral hypercube." This setup facilitates comparative analysis of synthesized data within a unified coordinate system.

Measurement Setup

Based on an analysis of existing models for visible sky hemisphere radiation—particularly regarding the data required to construct radiation distributions under varying weather conditions—we propose an experimental measurement setup designed to capture both image data and associated metadata. This setup consists of three main components: a measurement module for acquiring image data and metadata, a positioning module to spatially orient the measurement module with respect to the hemisphere (determining the primary observation direction in azimuth and elevation coordinates), and a network element that facilitates data exchange among devices within a local network, acquires data from network API services, and stores measurement data in both a database and on an FTP server (Figure 3).

The system's components are managed and operated through Python, using a combination of open-source libraries and custom-built solutions specifically designed for data acquisition and preliminary processing. The primary control software coordinates the measurement and positioning modules throughout the data collection process. The modular, mobile design of the station allows deployment in various locations, and it is operated via a laptop for flexibility and ease of use.

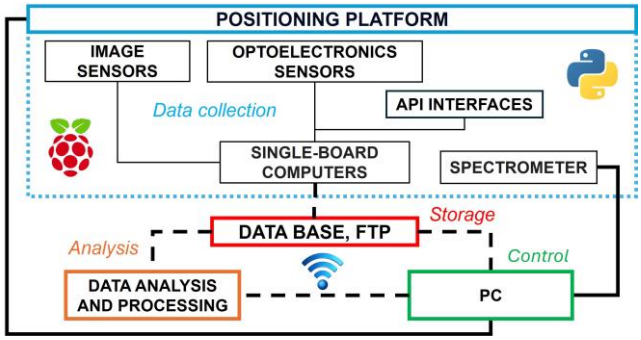

Fig. 3. The main components of the measurement setup

The measurement module includes both point sensors and image sensors. Point sensors capture data from a specific spatial direction, while image sensors provide 2D representations of the radiation distribution across the hemisphere from a given viewpoint.

The construction of the measurement component used the development of the following optoelectronic devices and components (Fig. 4):

- spectrometer CCD (3648 pixels, spectral range λ = 200 - 1100nm, spectral resolution <2nm) and fiber optic output with collimator (summary FOV ~ 10°),
- wide angle VIS camera (FOV = 220°),
- narrow angle camera with Arducam M2016ZH01 lens (focal length = 16mm).

The data acquisition within the measurement module is supplemented by the recording of local and instantaneous values of basic parameters under measurement conditions by the environmental module with sensors:

- digital ambient light sensor TSL25911FN
- UV sensor LTR390-UV-1,
- VOC sensor - SGP40VOC,
- temperature, humidity and air pressure sensor - BME280.

The data acquisition within the measurement module is supplemented by the recording of local and instantaneous values of basic parameters under measurement conditions by the environmental module. The system's modular configuration and sensor management are facilitated through dedicated microcontrollers and a central system controller, which coordinates module operation within an AdHoc local network established for device communication.

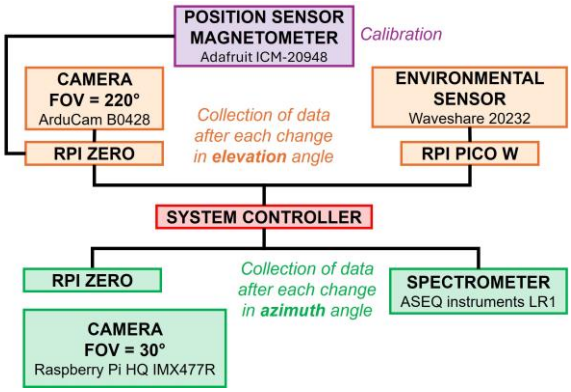

Fig. 4. Measurement component

To enable hemispherical mapping, a structure was designed to allow precise adjustments in both azimuth and elevation of the measurement components' observation direction.

In the developed setup, the positioning component consists of two rotational stages, which control the azimuth and elevation angles for each measurement point during data acquisition.

The orthogonal arrangement of these stages forms a standard pan-tilt platform. Key components include motors with integrated controllers and an Adafruit BNO085 orientation sensor, an IMU equipped with a 3-axis accelerometer, magnetometer, and gyroscope.

This sensor provides the necessary raw 9-DoF data (from the accelerometer, magnetometer and gyroscope) such as magnetic north orientation and absolute spatial orientation. These data are critical for calibration and monitoring operational parameters during measurements (Fig. 5).

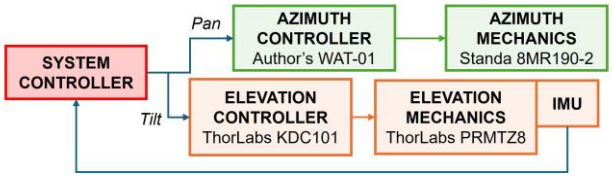

Fig. 5. Positioning component.

Given the modular sensor management requirements, the need for data storage on publicly accessible network resources, and the potential for acquiring supplementary environmental metadata from external API services, the implementation it was proposed to implement a network component. This setup establishes an AdHoc local network that connects to the global network via router equipped with a 5G modem, enabling the seamless operation of various sensors within the measurement system. The router is configured to assign fixed IP addresses to each component of the measurement station, facilitating network communication and online operation capabilities. This configuration allows measurement data to be transferred to publicly accessible resources, which is particularly useful for field measurements The overall structure of the proposed network solution is depicted in Figure 6.

With internet access, environmental data are further supplemented with information from the https://open-meteo.com API, which provides location- and time-specific parameters. These include cloud cover percentage (%), proportions of high, medium, and low cloud cover (%), global horizontal irradiance (W/m²), hourly averaged direct solar radiation power density on both horizontal and normal planes (W/m²), daily averaged diffuse solar radiation (W/m²), total daily terrestrial radiation density (W/m²), and the daily maximum UV index.

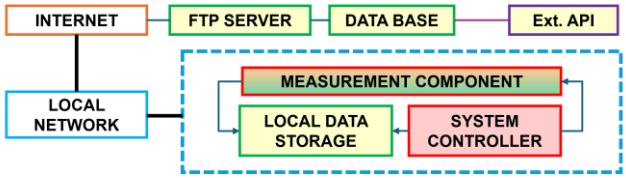

Fig. 6. Network component

"Point" data, such as temperature, pressure, humidity, VOC, and UVC, are recorded directly into a database, while more complex data structures—1D data from the spectrometer and 2D data from VIS cameras—are stored on an FTP server as text files, JSON files, or image files, respectively. Each file is labeled with a timestamp and a data source prefix in its filename to facilitate identification during analysis. The FTP directory structure is organized by data type/source, and the names of generated files are logged in the database. The final configuration of the experimental measurement station is presented in Figure 7.

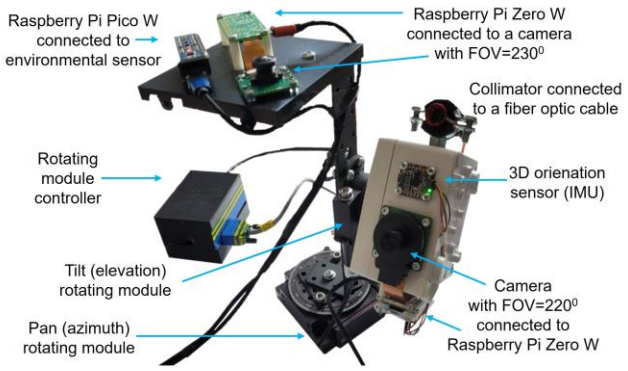

Fig. 7. Set up - measurement and positioning components

The measurement station enables the design of custom scanning paths across the hemisphere and allows control over the resolution of both spectral and image data collection. The scan area and step size can be parameterized individually for each axis (azimuth and elevation). In its default mode, the system is set to scan the entire visible hemisphere (i.e., ΔAz = 360°, ΔEl = 90°). All measurement data are initially acquired and stored in the memory of the main system controller. When an online network connection is available, data are uploaded to a public server (with portions directed to a database and others to an FTP server). For offline measurements, data are transferred once a public network connection becomes available. To optimize storage resources, data uploaded to an external server can be deleted from the system controller's memory.

Accurate data acquisition requires that the device's geographic position and spatial orientation are established before beginning a measurement session. This process includes leveling the device and aligning it to geographic north, which constitutes spatial calibration. This calibration uses the integrated Pan-Tilt IMU orientation sensor, GPS data, and network-provided magnetic declination corrections to determine the geographical north. Conducting this calibration is essential for comparing data across different sessions and aligning results with mathematical models.

Test Measurements and Characteristics

The developed station supports measurements in various configurations, including different hemisphere areas, spherical resolution, and sensor data scopes. This paper presents results from a sample measurement session in which the entire hemisphere was scanned with a relatively coarse angular step of 10° in both azimuth and elevation. These measurements were conducted under clear skies on July 16, 2024, between 10:37 and 11:05, on the observation terrace of the IOE WAT (Fig. 8).

The measurement process involves sequentially adjusting the angular parameters of the sensors observation directions according to a predefined scanning path and step size. This is achieved by precise control of the positioning component. Once the mechanism reaches the target position, each sensor acquires its respective set of data.

The collected data are archived locally and, if a connection to a public network is available, transmitted to a database and FTP server. A local network is also established, enabling real-time monitoring of the data

acquisition process, including online access to the video feed from the measurement station's cameras.

Below is an example of data from a measurement session—a dataset recorded at 10:38 (Fig. 9).

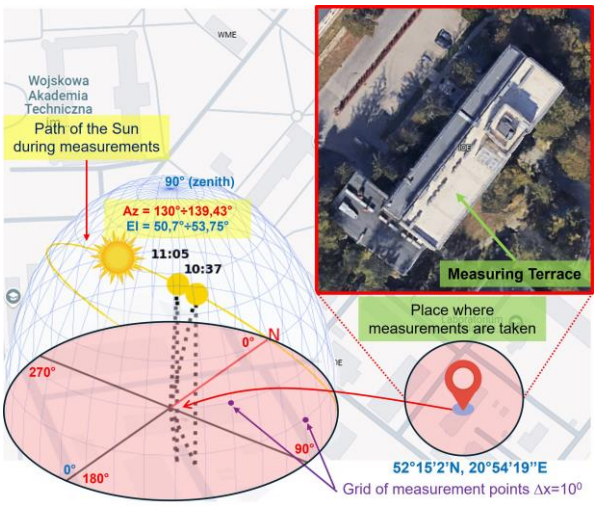

Fig. 8. Place and Conditions for Measurement Execution

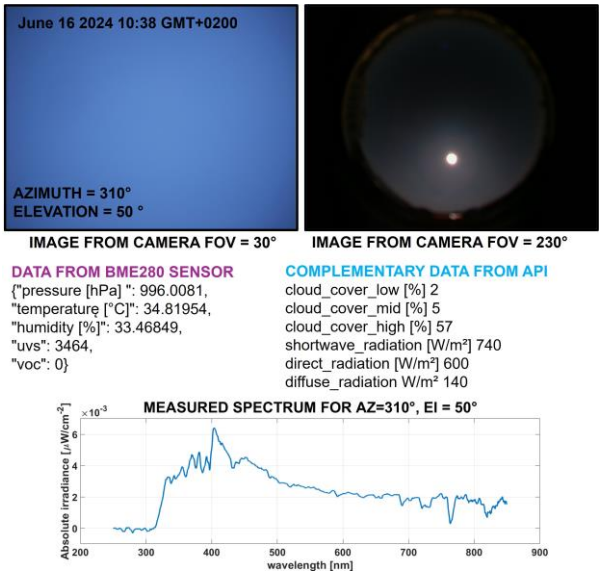

Fig. 9. Example of RAW measurement data set

Complementing the real measurements are data derived from a sky diffuse radiation model [1,7]. The calculations for a clear-sky spectrum are based on the SPCTRAL2 algorithm, as published in [1] and implemented by the authors in MATLAB. The software first determines the Earth-Sun correction factor based on the date and time to be modeled. This factor accounts for the variation in solar intensity due to changes in the Earth-Sun distance throughout the year. Next, the program reads tabulated extraterrestrial spectral irradiance values and maps them to the required wavelengths, followed by the calculation of spectral intensity.

Subsequently, the solar position angles (elevation and azimuth angles) relative to the detector's location—specified by the latitude and longitude of the measurement station—are computed. Based on the solar zenith angle, the air mass is calculated to estimate the transmission of both direct and diffuse sunlight through the Earth's atmosphere. Atmospheric conditions are characterized by parameters such as atmospheric pressure, aerosol optical thickness at 500 nm, water vapor content, ozone content, and surface albedo, which influences the intensity of diffuse radiation. Spectral direct irradiance refers to sunlight that has not been scattered by the atmosphere, while diffuse irradiance represents sunlight scattered by the atmosphere, and global (or total) irradiance is the sum of direct and diffuse sunlight (Fig. 10).

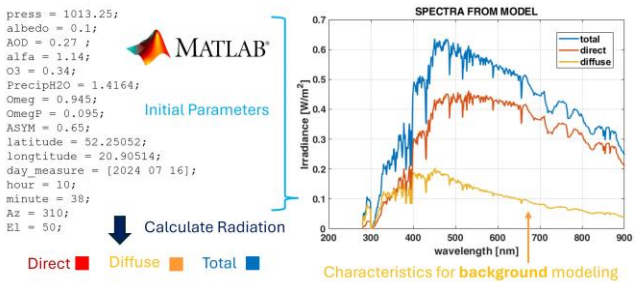

Fig.10. Modeling of Sky Hemisphere Radiation in MATLAB: Spectral Distribution of Radiation Components at Specific Locations, Times, and Measurement Points on the Hemisphere (Azimuth, Elevation)

The data presented above represent only a small portion of the extensive dataset acquired and synthesized throughout the entire measurement session. Based on these data, selection and preliminary processing are conducted, followed by more advanced and complex analyses.

Source Data Processing and Analysis

The primary data sources gathered through the developed measurement system include spectral data and visual material from imaging sensors. While other data sources provide a supplementary function, they are critical for the accurate interpretation of the primary data and will play an essential part in future work with models of sky hemisphere diffuse radiation, facilitating comparison of synthesized data against actual measurements.

The sample measurement data presented in the previous section were intended to illustrate the general types of data handled by the measurement and analysis system. Below, we outline selected aspects of source data processing and analysis, which are the current focus of the research.

A significant aspect of data analysis involves correlating spectral data with image material acquired from imaging sensors. The design of the measurement setup, along with the data acquisition approach, facilitates data synthesis from various sources without the need for image alignment procedures. However, for effective comparative analysis, raw data must be converted into a common hemispherical coordinate system. For input data processing, this necessitates synthesizing a panoramic view from conventional fisheye images and constructing a HyperCube structure from the spectral data series.

Data acquired from a fisheye camera can be converted into an equivalent panoramic representation. However, to ensure reliable results when comparing panoramic imagery with synthesized spectral images, an accurate calibration process is required on the measurement setup. This includes aligning the image's primary axis with the spectrometer's observation axis, positioning the camera on the rig to ensure the image's central point indicates zenith, and leveling the platform.

Converting fisheye data into a panoramic format is an image processing challenge that involves defining the

angular field of view of the wide-angle camera to match the angular range of the spectrometer data. The prepared image is then geometrically transformed into a panorama. Mathematically, this transformation is referred to as "fisheye-to-panoramic." In a fisheye image, each point (x_f,y_f) corresponds to a 3D point on the spherical projection of the real scene. In equiangular projection, azimuth and elevation map directly to the horizontal and vertical pixel coordinates (x_p,y_p). The stages of converting a fisheye image into a panoramic image are shown in Figure 11 and expressed by the following equations:

(1) $$x_p = \frac{W_p(\phi + \pi)}{2\pi}$$

(2) $$y_p = \frac{H_p\theta}{\pi}$$

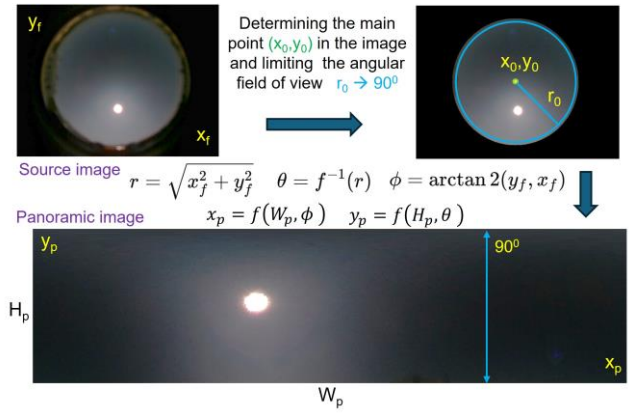

Fig. 11. Fisheye image processing for panoramic representation

Such an image representation, where columns *x* correspond to azimuthal angles and rows *y* to elevation angles, presents the overall structure of the measurement process, making it a useful foundation for comparison with other data collected throughout the measurement session.

Based on the set of spectral data obtained for different angular coordinates of the hemisphere (azimuth, elevation), it is possible to synthesize a structure known as the hyperspectral cube. This structure comprises a 3D dataset with two spatial dimensions (azimuth, elevation - denoted as *x, y)* and one spectral dimension (wavelength - *λ*). Each pixel in the 2D angular domain has a corresponding spectral signature represented as a vector of irradiance values detected across various wavelengths. The hyperspectral cube can therefore be represented as a multidimensional array, where each element *I(x,y,λ)* denotes the irradiance value at angular coordinates *(x,y)* and wavelength *λ*. Given a set of pointwise spectral measurements on a rectangular grid from the hemisphere (azimuth, elevation), the construction of a hyperspectral cube can be mathematically described as follows:

Assuming the measurements consist of:

- a 2D grid of angular coordinates on the hemisphere (x_i,y_j) for $i=1,2,...,N_x$ i $j=1,2,...,N_y$, where N_x and N_y are the number of grid points in the azimuth and elevation directions,
- at each point (x_i,y_j), a spectral measurement is performed, yielding a value $A(x_i,y_j,\lambda_k)$ at various wavelengths λ_k, where $k=1,2,...,N_\lambda$, and N is the number of discrete wavelength values.

The hyperspectral cube $I(x,y,\lambda)$ can thus be represented as a 3D array or tensor with dimensions $Nx \times Ny \times N\lambda$, where $I(i,j,k)$ is the irradiance value for the angular position(x_i,y_j) and wavelength λ_k. In this framework, the hyperspectral cube functions as a 3D data structure essential for multidimensional spectral analysis.

(3) $$I(x_i, y_j, \lambda_k) = A(x_i, y_j, \lambda_k)$$

The synthesized data, such as panoramic images and spectral images (as an XY_λ slice from the hyperspectral cube), can be compared with each other, as the corresponding structures/points on both images are aligned. In this case, "image registration" within a common coordinate system (as the algorithmic process of finding the transformation between images) is not required. Image alignment is performed hardware-wise through proper calibration of the setup, i.e., correct positioning of components relative to each other, as well as leveling the system and orienting it relative to geographical north. On such prepared images (or their fragments), similarities and differences can be explored, and if necessary, image resolution conversion can be carried out.

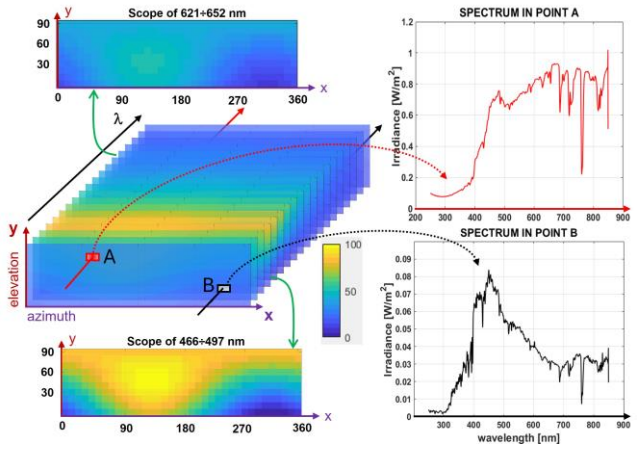

Fig. 12. Hypercube synthesis based on a series of spectral data acquired from observations of the sky hemisphere.

Issues such as those presented, for example, in Figure 13, are crucial from the perspective of finding ways to incorporate weather parameters into the sky hemisphere model as a measurement background.

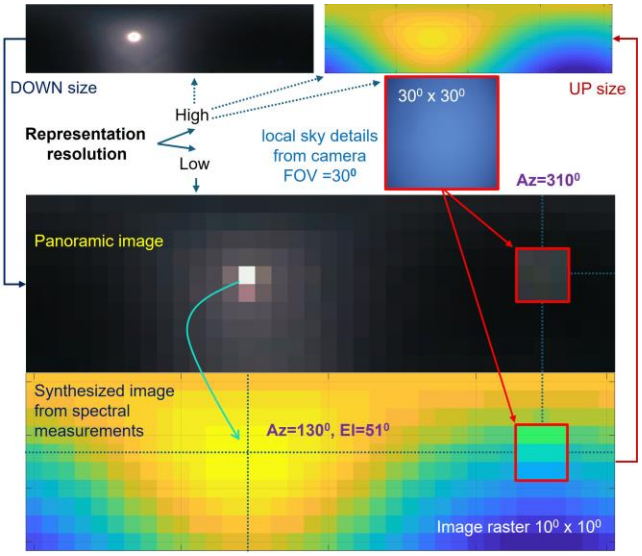

Fig. 13. Full correspondence between panoramic image and synthesized spectral image.

Summary

The acquisition of information regarding the spectral distribution of radiation from the sky hemisphere is of significant interest across various disciplines, driving extensive research on modelling this radiation over the past several decades. Today, numerous well-established mathematical models are commonly used in fields such as renewable energy and satellite remote sensing. However, from the perspective of utilizing spatial distribution data of this radiation as a background for visual analysis, the data synthesized by these models does not fully meet the authors' expectations. This gap has led to the development of a low-cost system designed to acquire spectral and imaging data of the sky hemisphere. The goal was to create a mobile and highly automated measurement platform capable of conducting measurements at different locations, times of day, and under varying environmental conditions.

The system presented in this study includes a measurement platform and experimental device, primarily based on simple and affordable sensors to monitor real-time dynamics in solar radiation intensity. With this solution, the authors aim to establish a reconfigurable 2D model (azimuth, elevation) of diffuse hemispheric radiation to support imaging analyses. The central research question is whether datasets derived from point and 2D sensors monitoring the sky hemisphere can be used to modify data from existing mathematical models, such that they can be integrated to synthesize measurement backgrounds for simulation studies. These studies may involve dynamically generated scenes across selective spectral ranges (from UV to NIR) and, ultimately, support real-world visual analyses.

The developed platform and measurement system represent an initial experimental approach to this topic. Key advantages include remote measurement management, data acquisition, and cloud-based storage. Preliminary testing across various measurement sessions has validated the proposed solution, particularly with respect to the mechanical positioning, sensor data acquisition, and storage, as well as the accuracy of data processing and analysis. The results presented in this article—showcasing the synthesis and processing of images from various sources and their analysis within a common coordinate framework—demonstrate the effectiveness of this approach. Furthermore, the obtained data provide a foundational basis for advancing analytical work, with the potential to modify the mathematical model using real-world measurement data, potentially incorporating artificial intelligence methods

Praca została sfinansowana w ramach projektu NCBiR w konkursie SZAFIR. This work was funded by the NCBiR project under the SZAFIR program.

***Authors**: mgr inż. Aleksandra Kucharczyk - Drab, Wojskowa Akademia Techniczna, Instytut Optoelektroniki, ul. gen. S. Kaliskiego 2, 00-908 Warszawa, E-mail: aleksandra.kucharczyk@wat.edu.pl;*
mgr inż. Radosław Ryniec, Wojskowa Akademia Techniczna, Instytut Optoelektroniki, ul. gen. S. Kaliskiego 2, 00-908 Warszawa, E-mail: radoslaw.ryniec@wat.edu.pl;
dr hab. inż. Marek Piszczek, profesor WAT, Wojskowa Akademia Techniczna, Instytut Optoelektroniki, ul. gen. S. Kaliskiego 2, 00-908 Warszawa, E-mail: marek.piszczek@wat.edu.pl;

REFERENCES

[1] Bird, Richard E., and Carol Riordan. "Simple solar spectral model for direct and diffuse irradiance on horizontal and tilted planes at the earth's surface for cloudless atmospheres." Journal of climate and applied meteorology (1986): 87-97
[2] Xie, Yu, and Manajit Sengupta. "A fast all-sky radiation model for solar applications with narrowband irradiances on tilted surfaces (FARMS-NIT): Part I. The clear-sky model." *Solar Energy* 174 (2018): 691-702
[3] Xie, Yu, Manajit Sengupta, and Chenxi Wang. "A fast all-sky radiation model for solar applications with narrowband irradiances on tilted surfaces (FARMS-NIT): Part II. The cloudy-sky model." Solar Energy 188 (2019): 799-812
[4] Xie, Yu, and Manajit Sengupta. "Fast All-sky Radiation Model for Solar Applications (FARMS): A Brief Overview of Mechanisms, Performance, and Applications." (2016)
[5] Ya'u, Muhammad Jamilu, et al. "Global solar radiation models: A review." Journal of photonic materials and technology 4.1 (2018): 26-32
[6] Prieto, Jesús-Ignacio, and David García. "Global solar radiation models: A critical review from the point of view of homogeneity and case study." Renewable and Sustainable Energy Reviews 155 (2022): 111856
[7] Gueymard, Christian A. "The SMARTS spectral irradiance model after 25 years: New developments and validation of reference spectra." Solar Energy 187 (2019): 233-253.
[8] Chu, Tsai-Ping, et al. "Estimation of solar irradiance and solar power based on all-sky images." Solar Energy 249 (2023): 495-506
[9] Boland, John, Jing Huang, and Barbara Ridley. "Decomposing global solar radiation into its direct and diffuse components." Renewable and Sustainable Energy Reviews 28 (2013): 749-756
[10] El Mghouchi, Y., et al. "Comparison of three solar radiation models and their validation under all sky conditions–case study: Tetuan city in northern of Morocco." Renewable and Sustainable Energy Reviews 58 (2016): 1432-1444
[11] Chen, Shanlin, et al. "Global and direct solar irradiance estimation using deep learning and selected spectral satellite images." Applied Energy 352 (2023): 121979
[12] Gueymard, Christian A., and Miroslav Kocifaj. "Clear-sky spectral radiance modeling under variable aerosol conditions." Renewable and Sustainable Energy Reviews 168 (2022): 112901
[13] Del Rocco, Joseph, et al. "Real-time spectral radiance estimation of hemispherical clear skies with machine learned regression models." Solar Energy 204 (2020): 48-63
[14] Maskarenj, Marshal, Rangan Banerjee, and Prakash C. Ghosh. "Design and development of a low-cost angular sky luminance measurement system." Building and Environment 142 (2018): 22-33
[15] Sánchez-Segura, César D., et al. "Solar irradiance components estimation based on a low-cost sky-imager." Solar Energy 220 (2021): 269-281
[16] Alonso-Montesinos, J., and F. J. Batlles. "The use of a sky camera for solar radiation estimation based on digital image processing." Energy 90 (2015): 377-386
[17] Xu, Guoning, et al. "Measurements and analysis of solar spectrum in near space." Energy Reports 9 (2023): 1764-1773